

# Predictable nonwandering localization of covariant Lyapunov vectors and cluster synchronization in scale-free networks of chaotic maps

Pavel V. Kuptsov<sup>1,\*</sup> and Anna V. Kuptsova<sup>1</sup>

<sup>1</sup>*Institute of electronics and mechanical engineering,  
Yuri Gagarin State Technical University of Saratov, Politekhnikeskaya 77, Saratov 410054, Russia*  
(Dated: September 29, 2018)

Covariant Lyapunov vectors for scale-free networks of Hénon maps are highly localized. We revealed two mechanisms of the localization related to full and phase cluster synchronization of network nodes. In both cases the localization nodes remain unaltered in course of the dynamics, i.e., the localization is nonwandering. Moreover this is predictable: the localization nodes are found to have specific dynamical and topological properties and they can be found without computing of the covariant vectors. This is an example of explicit relations between the system topology, its phase space dynamics, and the associated tangent space dynamics of covariant Lyapunov vectors.

PACS numbers: 05.45.-a, 05.45.Xt, 05.45.Jn, 89.75.Hc

## I. INTRODUCTION

Localization properties of Lyapunov vectors in spatio-temporal chaotic systems attract a permanent interest since the early works till the present days [1–4]. Recently it has been renewed due to the discovery of algorithms for covariant Lyapunov vectors (CLVs) [5, 6]. The evolution of these vectors is governed by linear equations under chaotic forcing, so that their localization can be treated as a sort of Anderson localization [2]. The localization sites indicate unstable areas of a system, that, in particular, is important for atmosphere dynamics prediction [7]. For homogeneous systems the localization sites of the covariant vectors wander irregularly so that their dynamics can be described by stochastic equation of Kardar-Parisi-Zhang [8, 9]. In contrast, the localization positions in inhomogeneous systems are pinned at certain fixed positions [10].

In this paper we analyze properties of CLVs for scale-free networks of chaotic maps. We show that due to the presence of cluster synchronization the CLVs are localized. The first mechanism of the localization is related to the full synchronization clusters, and second one appears due to the existing of large phase synchronized clusters. Both of the localizations are nonwandering, i.e., nonzero sites of the vectors remain unchanged in course of the dynamics. Moreover these nodes have specific topological and dynamical properties so that they can be identified without computing the CLVs. This is an example of explicit relations between the system topology, its phase space dynamics, and the associated tangent space dynamics of CLVs.

The paper is organized as follows. In Sec. II we introduce the considered network and discuss its dynamics. Section III describes the structure of the tangent space of the network. The mechanism of CLVs localization on clusters of full synchronization is described in Sec. IV,

and in Sec. V we discuss the localization related to phase clusters. Finally, Sec. VI summarizes the paper results.

## II. MODEL SYSTEM AND CLUSTER SYNCHRONIZATION

### A. Dynamical network equations and network structure

We consider a network of Hénon maps build as a generalization of the Hénon chain from Ref. [11]:

$$\begin{aligned}x_n(t+1) &= \alpha - [x_n(t) + \epsilon h_n(t)]^2 + y_n(t), \\y_n(t+1) &= \beta x_n(t),\end{aligned}\quad (1)$$

$$h_n(t) = \sum_{j=1}^N \frac{a_{nj}}{k_n} x_j(t) - x_n(t), \quad k_n = \sum_{j=1}^N a_{jn}, \quad (2)$$

where  $N$  is the number of network nodes,  $t = 0, 1, 2, \dots$  is discrete time,  $a_{nj} \in \{0, 1\}$ ,  $a_{nn} = 0$  are the elements of the  $N \times N$  adjacency matrix  $\mathbf{A}$ , and  $k_n$  is degree of the  $n$ th node, i.e., the number of its connections.  $\alpha = 1.4$  and  $\beta = 0.3$  are the parameters, controlling local dynamics, and  $\epsilon \in [0, 1]$  is the coupling strength. The system is time-reversible:  $x_n(t) = y_n(t+1)/\beta$ ,  $y_n(t) = -\alpha + [y_n(t+1) + \epsilon h'_n(t+1)]^2/\beta^2 + x_n(t+1)$ , where  $h'_n(t) = \sum_{j=1}^N \frac{a_{nj}}{k_n} y_j(t) - y_n(t)$ .

We consider random networks with scale-free structure generated via a stochastic process described in Ref. [12]. The process starts from two linked nodes. At each iteration we add one node to the network and one link connecting it with one of the existing nodes. The node to connect is chosen at random with probability that is proportional to its connectivity degree  $k_n$ , i.e., via so called preferential attachment mechanism. After  $N - 1$  steps we obtain a network with  $N$  nodes and  $N - 1$  connections. The node degree distribution for such networks has a power law shape  $P(k) \sim k^{-3}$ . An example of the network is shown in Fig. 5 (this figure is discussed in detail below).

\* Corresponding author. Electronic address: [p.kuptsov@rambler.ru](mailto:p.kuptsov@rambler.ru)

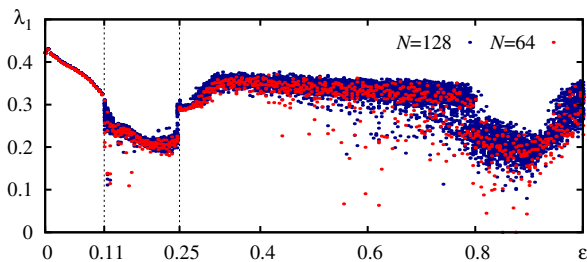


Figure 1. (color online) The first Lyapunov exponent vs.  $\epsilon$  for  $N = 128$  and  $64$ . Each point is computed independently with a new matrix  $\mathbf{A}$  and initial conditions. At  $N = 128$  and  $64$  there are 50 and 5 points, respectively, for each  $\epsilon$ . Lines at  $\epsilon = 0.11$  and  $0.25$  delimit the area of interest.

By construction, the networks under consideration do not have loops. It means that starting from any node one can not return to it without moving back. The networks always have a lot of star-like structures when one hub node is connected with many subordinate ones, like, for example, node 10 in Fig. 5. Moreover these structures can form a hierarchy, see the hub node 11 that is subordinate with respect to node 10. The structure of considered networks is essentially inhomogeneous. Usually a few nodes are connected with very many others, and many nodes have only one link. All of these properties are found to result in a very long transient time required for the network to arrive at stationary regime. This will be discussed in Sec. IID.

### B. The largest Lyapunov exponent

The dynamics of the network (1) is, in general, chaotic. To characterize it we compute Lyapunov exponents using the standard algorithm suggested in Refs. [13, 14] (see also Ref. [15] for a review).

Figure 1 shows the largest Lyapunov exponent  $\lambda_1$  at different coupling strengths. At  $\epsilon < 0.11$  the exponent unambiguously depends on  $\epsilon$  regardless of the network matrix  $\mathbf{A}$ , initial conditions, and the network size. This occurs because the nodes interact weakly with each other, so that the detailed network structure is not very important. The nodes within this area do not demonstrate any concerted oscillations. The area  $0.11 < \epsilon < 0.25$  clearly differs from all others. The dependence  $\lambda_1(\epsilon)$  is ambiguous here: every new combination of the network matrix  $\mathbf{A}$  and initial conditions are characterized with their own  $\lambda_1$ . Another feature of this area is lower values of  $\lambda_1$  with respect to the surrounding areas. This is due to the cluster synchronization emerging here, see the discussion below in Sec. IIC. The dependence  $\lambda_1(\epsilon)$  remain ambiguous at  $\epsilon > 0.25$ , though the exponents becomes higher. At  $\epsilon > 0.8$  the exponents again becomes lower so that this area is similar to the marked area  $0.11 < \epsilon < 0.25$ .

In what follows we shall restrict ourselves with the area  $0.11 < \epsilon < 0.25$ .

### C. Full and phase cluster synchronization

Though the synchronization of the whole network is not observed, the nodes can form clusters of synchronized oscillations. Both full and phase synchronization is possible. The former stands for the equivalence of variables at the synchronized nodes, and the latter implies the coincidence of positions of minima and maxima of synchronized time series. The fully synchronized nodes will be referred to as FS-clusters, and phase synchronized nodes will be called Ph-clusters.

The phase cluster synchronization of networks nodes is studied in Ref. [16]. According to the approach suggested there, one can detect the Ph-clusters computing phase distances. Given a starting time  $t_0$  and a time interval  $\mathcal{T}$ , count at  $t_0 \leq t < t_0 + \mathcal{T}$  the numbers  $\nu_m$  and  $\nu_n$  of local minima of  $x_m(t)$  and  $x_n(t)$ , respectively, and also find the number  $\nu_{mn}$  of simultaneous minima of  $x_m$  and  $x_n$ . Then the phase distance is computed as

$$d_{mn} = 1 - \nu_{mn} / \max(\nu_m, \nu_n). \quad (3)$$

When it vanishes all the minima of  $x_m$  and  $x_n$  occur simultaneously and this is the case of phase synchronization of  $m$ th and  $n$ th nodes over the time interval  $\mathcal{T}$ . To identify the Ph-clusters one can build an auxiliary graph whose  $n$ th and  $m$ th nodes are linked if  $d_{mn} = 0$  and find the clusters as connected components of this graph.

Nonzero  $d_{mn}$  is a fraction of time when the nodes  $m$  and  $n$  are not synchronized. Thus the minimum of  $d_{mn}$  over  $n$ , i.e.,

$$\tilde{d}_m = \min\{d_{mn} | n = 1 \dots N\}, \quad (4)$$

can be treated as degree of the desynchronization of the  $m$ th node with the rest of the network.

The FS-clusters can be identified using the matrix of mean absolute differences between dynamical variables over the computation interval  $\mathcal{T}$ :

$$q_{mn} = \sum_{t=0}^{\mathcal{T}-1} |x_m(t_0 + t) - x_n(t_0 + t)| / \mathcal{T} \quad (5)$$

The FS-clusters correspond to connected components of an auxiliary graph whose  $m$ th and  $n$ th nodes are connected when  $q_{mn} = 0$ . In actual numerical simulations we considered two nodes as synchronized if  $q_{mn} < 10\epsilon_m$ , where  $\epsilon_m \approx 10^{-16}$  is the machine epsilon for double precision variables that was employed.

The length of the interval  $\mathcal{T}$  for which the cluster detection is performed can influence the resulting picture. As we discuss in this section below and in Sec. IID, there exist so called floating nodes that intermittently can either belong to one of the Ph-clusters or oscillate separately. With a large  $\mathcal{T}$  we consider clusters including

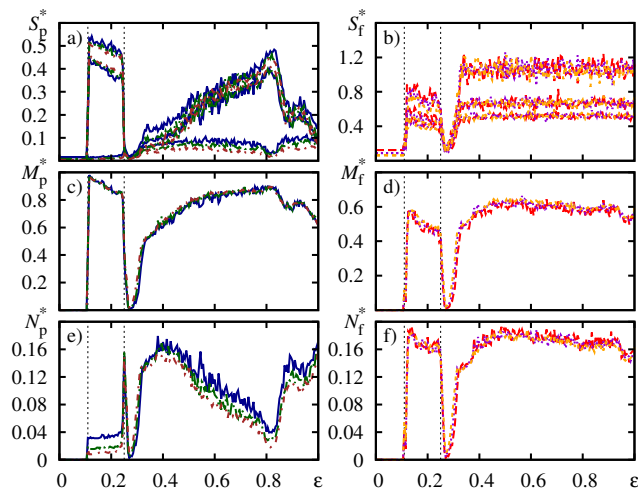


Figure 2. (color online) (a,b) Rescaled sizes of three largest Ph- and FS-clusters, see Eq. (6). (c,d) Rescaled numbers of nodes attached to all Ph- and FS-clusters, see Eq. (7). (e,f) Rescaled numbers of Ph- and FS-clusters, see Eq. (8). All values are averaged over 25 computations with different matrices  $\mathbf{A}$  and initial conditions at each  $\epsilon$ .  $\mathcal{T} = 10000$ . Different curves in each panel correspond to  $N = 62, 128$ , and  $256$ . Vertical dotted lines are plotted at  $\epsilon = 0.11$  and  $0.25$  to delimit the area of interest.

only permanent nodes, while performing a serial cluster detections with a small  $\mathcal{T}$  we can take into account fluctuations arising due to the floating nodes.

Figure 2 illustrates the cluster synchronization of networks with  $N = 64, 128$ , and  $256$  nodes that is observed at different  $\epsilon$ . Panels (a) and (b) show rescaled sizes

$$S_p^* = S_p/N, \quad S_f^* = S_f/\sqrt{N} \quad (6)$$

of three largest Ph- and FS-clusters, respectively. Panels (c) and (d) represents rescaled numbers

$$M_p^* = M_p/N, \quad M_f^* = M_f/N \quad (7)$$

of nodes attached to all Ph- and FS-clusters, respectively. Panels (e) and (f) show rescaled numbers

$$N_p^* = N_p/N, \quad N_f^* = N_f/N \quad (8)$$

of Ph- and FS-clusters, respectively. The clusters appears at  $\epsilon = 0.11$ . As one can see in panel (a) in the area  $0.11 < \epsilon < 0.25$  there are two large Ph-clusters whose relative sizes are  $S_p^* \approx 0.4 \div 0.5$ . The curves in panel (e) plotted for different  $N$  do not coincide, but not rescaled curves  $N_p$  do so (not shown), i.e., the number of Ph-clusters does not depend on  $N$ . Since  $S_p \sim N$ , see Eq. (6), regardless of  $N$  these clusters includes the bulk of nodes. However, as follows from panel (c) and Eq. (7), the Ph-clusters includes at any  $N$  approximately 85% of nodes, so that always there are nodes not synchronized with Ph-clusters.

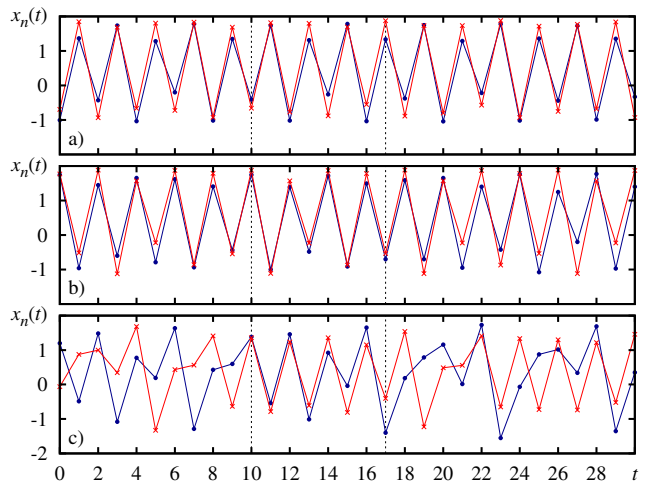


Figure 3. (a,b) Oscillations at nodes belonging to two large Ph-clusters. (c) Separated nodes not synchronized with others. Vertical dotted lines delimit the interval when both separated nodes in panel (c) are attached to the cluster represented in panel (b).  $N = 128$ ,  $\epsilon = 0.17$ .

Despite the Ph-clusters, the number of FS-clusters scales as  $N_f \sim N$  and also the total number of nodes attached to all FS-cluster grows as  $M_f \sim N$ . It presumes that the mean size of FS-nodes is constant. However the size of the largest cluster grows: at  $N = 64, 128$ , and  $256$  the sizes are  $S_f \approx 6, 9$ , and  $13$ , respectively. According to Eq. (6), the sizes of the largest FS-clusters scales with  $N$  as  $S_f \sim \sqrt{N}$ .

At the right boundary of the discussed area at  $\epsilon = 0.25$  the large Ph-clusters desintegrate into many small ones, see the spike of  $N_p^*$  in the panel (e). Moreover, in this area  $N_p$  starts to scale as  $N_p \sim N$ . As  $\epsilon$  further grows all clusters disappears but then their number again increase. Notice the identical behaviour of curves in panels (c,e) and (d,f), respectively, around  $\epsilon \approx 0.3$ . It indicates the presence here of FS-clusters only. Subsequent growth of  $\epsilon$  results in reappearing of the Ph-clusters, but their number is still high. At  $\epsilon \approx 0.4$  the number of Ph-clusters starts to decay, panel (e), and the number of the attached nodes increases, panel (c). Also observe the growth of the first two largest clusters, panel (a). As for the FS-clusters, their sizes, panel (b), the number of attached nodes, panel (d), and their total number, panel (f), remains approximately unchanged. At  $\epsilon \approx 0.8$  one again observes the situation when there are two large Ph-clusters and many small FS-clusters. But contrary to the area  $0.11 < \epsilon < 0.25$ , this area is much narrower and when  $\epsilon$  gets larger the desintegration of Ph-clusters occurs within the wider range of  $\epsilon$ .

As already mentioned above, we shall consider the dynamics of the network within the area at  $0.11 < \epsilon < 0.25$ .

Figure 3 illustrates behaviour of synchronized and separated nodes, panels (a,b) and (c), respectively, within the area of interest, when almost all nodes belong to

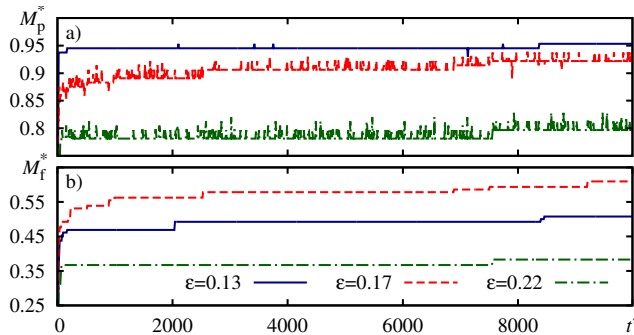


Figure 4. Convergence of the (a) Ph- and (b) FS-clusters.  $t'$  enumerates the cluster detection procedures performed over the intervals  $\mathcal{T} = 100$  in course of the evolution of the system.  $N = 128$ ,  $\epsilon = 0.13, 0.17$ , and  $0.22$ .

two large Ph-clusters. Observe in panels (a) and (b) strict alternations of maxima and minima of variables attached to Ph-clusters and irregular variations of their amplitudes. Also compare the panels (a) and (b): the oscillations of Ph-clusters have opposite phases. The separated nodes, panel (c), oscillate irregularly, however for some time they can be attached to one of the clusters, see area  $25 < t < 30$  in panel (c).

If a node spends an essential part of time being synchronized with others however can lose intermittently the synchronization, it will be called a floating, according to the notation suggested in Ref. [16].

#### D. Convergence of the cluster structure

The network (1) converges very slowly to its stationary regime. As one can see in Fig. 4, the relative numbers  $M_p^*$  and  $M_f^*$  of nodes attached to Ph- and FS-clusters, respectively, can change even after a very long evolution time. Since in this figure the clusters are identified over the intervals  $\mathcal{T} = 100$ , the total evolution time of the system is  $t = 10^6$ . The represented examples are not very typical in a sense that we tried approximately ten different matrices  $\mathbf{A}$  and initial conditions for each  $\epsilon$  to show the cases with the worst convergence. However, the convergence in other cases is not much faster. Nevertheless, both in Fig. 4 and in all other cases we tried the curves always behaved as if they approached to limiting values. Thus we can conjecture that the stationary regime exists and take a long transient time to approach it,  $t_{\text{trans}} = 5 \times 10^5 N/64$ .

Observe frequent peaks and dips on the curves for  $M_p^*$ , see Fig. 4(a). They appear due to the floating nodes that intermittently attach and detach the Ph-clusters. The floating nodes exist only with respect to Ph-clusters; if a node gets attached to a FS-cluster it stays synchronized permanently, see Fig. 4(b).

Curves in Fig. 4(a) can be treated as a highly fluctuating signal. However, the observed fluctuations appear

due to the serial cluster detection with sufficiently short  $\mathcal{T}$ . One can change the definition of observable variables and perform the clusters detected just once over the whole computation time. The clusters defined in this way are stationary, but also there are non cluster nodes oscillating chaotically. Below we shall employ both approaches.

#### E. An example of the network

It is useful to enumerate the network nodes according to the cluster structure. First we find Ph- and FS-clusters and enumerate them with indexes  $i \in [0 \dots N_p]$  and  $j \in [0 \dots N_f]$ , respectively, in ascending order of their sizes, where  $N_p$  and  $N_f$  are the numbers of corresponding clusters. The index 0 indicates trivial clusters including a single node only. Then the nodes are assigned the indexes  $i_m$  and  $j_m$  in accordance to their membership in clusters, and also the desynchronization degree  $\tilde{d}_m$  is computed for them, see Eq. (4). Now the real-valued clustering index is defined as

$$\eta_m = \begin{cases} -\tilde{d}_m & \text{if } \tilde{d}_m > 0, \\ i_m + j_m / (N_f + 1) & \text{if } \tilde{d}_m = 0. \end{cases} \quad (9)$$

Finally, the nodes are enumerated in the ascending order of  $\eta_m$ . The negative  $\eta_m$  indicates that the corresponding node is not synchronized with others, and if in addition  $\eta_m$  is very close to zero the corresponding node is the floating one. The integer part of positive  $\eta_m$  is the index of Ph-cluster to which the node belongs and the fractional part encodes the FS-cluster index.

Figure 5 shows an example of the network structure as well as its Ph- and FS-clusters emerged in course of the evolution. The nodes are enumerated according to the ascending order of  $\eta_m$  that is plotted in Fig. 9(a). The cluster detection is performed over the whole computation interval  $10^5$ .

For this particular case there are five nodes that are not synchronized with others, i.e., have  $\eta_m < 0$ . The first two of them are essentially separated,  $\eta_{1,2} \approx -0.16$ , and the nodes 3, 4, and 5 are the floating ones with very small  $|\eta_m|$ :  $\eta_3 = -0.00054$ ,  $\eta_4 = -0.00028$ ,  $\eta_5 = -2 \times 10^{-5}$ .

The bulk of nodes form two large Ph-clusters. In our case for these clusters  $3 \leq \eta_m < 4$  and  $4 \leq \eta_m < 5$ , see Fig. 9(a). As one can see in Fig. 5, there is no any visible relation between the connectivity structure of the network and the locations of these clusters. The cluster nodes are mixed so that many nodes of the first cluster are connected with others only through elements of the second one and vice versa. As we mentioned above, see Fig. 3(a,b), the oscillations within these clusters have opposite phases. Thus, in a wider sense, one can say that all nodes of these two clusters are phase synchronized, but some with a phase shift.

Some of nodes of Ph-clusters are synchronized stronger so that they form FS-clusters embedded into Ph-clusters.

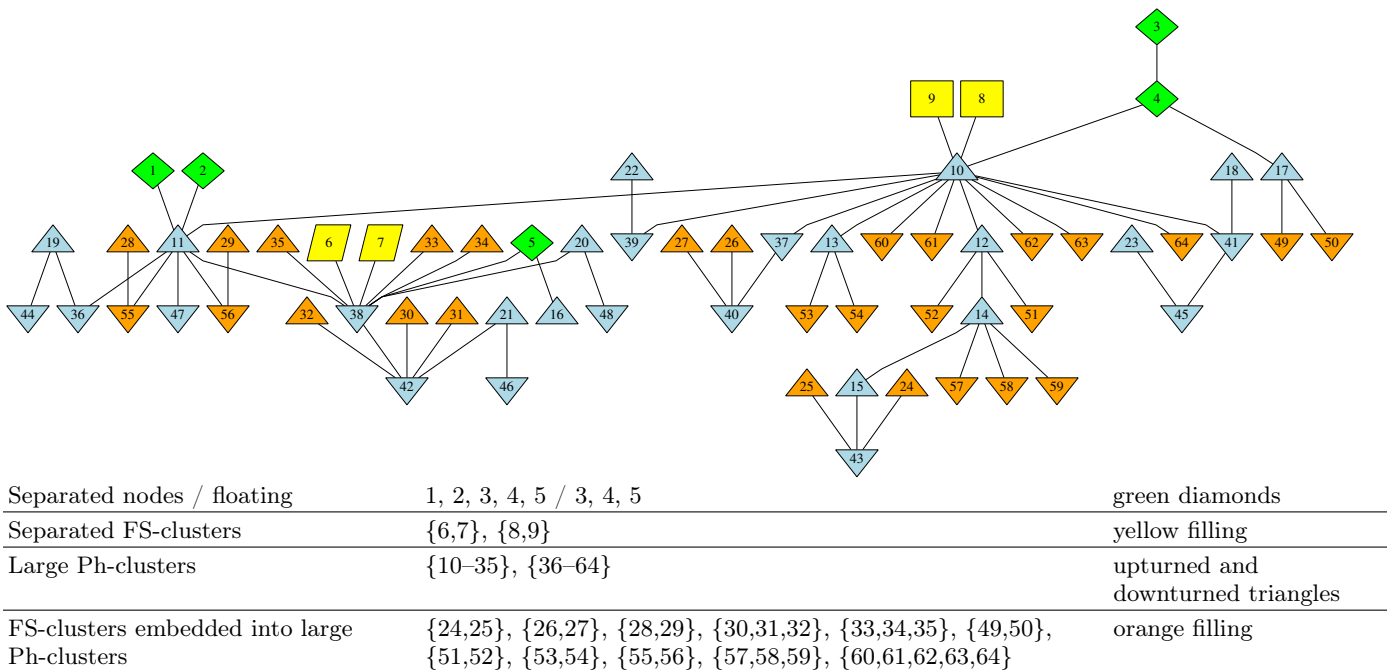


Figure 5. An illustration of the clustering of network (1) with  $N = 64$  and  $\epsilon = 0.17$ . The nodes and edges represent the connectivity structure and the shapes and colors of nodes indicate the states arrived in course of the evolution, see the table below the graph. To plot this figure we collected data for the cluster identification over  $\mathcal{T} = 10^5$  steps.

For these clusters  $\eta_m$  is fractional and  $\eta_m > 3$ . Observe that all of these clusters are formed by elements of star-like structures and all interactions inside FS-clusters pass through hub nodes. The hub nodes in turn are never synchronized with their subordinate nodes, see, for example the cluster  $\{24,25\}$  connected through a hub 43. Moreover, the hub always belongs to the opposite Ph-cluster: observe different orientations of the triangles representing the cluster nodes and the corresponding hubs. This type of synchronization was first reported in Ref. [16] for clusters of phase synchronization. The authors called it driven synchronization. Later this mechanism was independently described in Refs.[17, 18] and referred to as remote synchronization.

The structures mentioned so far are typical and always exist for any  $\mathbf{A}$  and initial conditions. In some cases, however, like for example the one shown in Fig. 5, several more small FS-clusters appear that are separated from two large Ph-clusters: the nodes 6 and 7 are fully synchronized with each other but are not embedded into Ph-clusters. The same is the case for the nodes 8 and 9.

Finally, notice that remote synchronization can also occur when “beams” of a star-like structure include two edges. The nodes 28 and 29 form a FS-cluster, but they can interact only through the nodes 55 and 56. The latter ones are also synchronized. The opposite orientation of the corresponding triangles indicates that these clusters are embedded into different Ph-clusters. This situation can be treated as remote synchronization of the second order.

### III. STRUCTURE OF THE TANGENT SPACE

#### A. The Jacobian matrix

The Jacobian matrix of the network (1) has a block form being composed of  $N \times N$  matrices:

$$\mathbf{J}(t) = \begin{pmatrix} \mathbf{F}(t) & \mathbf{I} \\ \beta \mathbf{I} & 0 \end{pmatrix}, \quad (10)$$

where

$$\begin{aligned} \mathbf{F}(t) &= -2\mathbf{G}(t) [(1 - \epsilon)\mathbf{I} + \epsilon\mathbf{K}^{-1}\mathbf{A}], \\ \mathbf{G}(t) &= \text{diag}\{x_n + \epsilon h_n\}, \quad \mathbf{K} = \text{diag}\{k_n\}, \end{aligned} \quad (11)$$

and  $\mathbf{I}$  is the identity matrix.  $\mathbf{J}(t)$  has a generic symplectic structure, i.e., at any  $t$  there exists a skew-symmetric matrix  $\mathbf{W}(t)$  such that  $\mathbf{J}(t)\mathbf{W}(t)\mathbf{J}(t)^T = -\beta\mathbf{W}(t)$ . Systems of this type were first introduced in Ref. [19], however unlike the referenced paper in our case  $\mathbf{W}(t)$  is a generic skew-symmetric matrix depending on  $t$ :

$$\mathbf{W}(t) = \begin{pmatrix} 0 & -\mathbf{Q}(t) \\ \mathbf{Q}(t) & 0 \end{pmatrix}, \quad (12)$$

where  $\mathbf{Q}(t)$  is a symmetric matrix such that the product  $\mathbf{F}(t)\mathbf{Q}(t) = \mathbf{M}(t)$  is also symmetric.  $\mathbf{Q}(t)$  can always be found since any matrix  $\mathbf{F}(t)$  can always be represented as the product of two symmetric matrices,

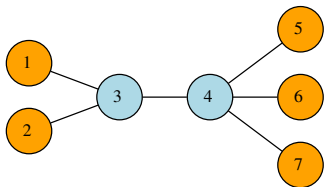


Figure 6. A toy network with two star-like structures. The orange color marks the nodes subjected to the remote synchronization.

$\mathbf{F}(t) = \mathbf{M}(t)\mathbf{Q}(t)^{-1}$  [20]. Due to this property the Lyapunov spectrum is symmetric [19]:

$$\lambda_n + \lambda_{N+1-n} = \log \beta \quad (13)$$

The Lyapunov spectra for our system are shown in Fig. 7 and discussed below.

### B. Pairwise orthogonal eigen-subspaces of the tangent space

In presence of FS-clusters the tangent space of the network (1) is split into  $N_f + 1$  time invariant subspaces that are pairwise orthogonal, where  $N_f$  is the number of FS-clusters. There are  $N_f$  subspaces representing perturbations transverse to manifolds where the FS-clusters belong, and the one that includes perturbations longitudinal to all of these manifolds.

Consider a toy  $7 \times 7$  network, see Fig. 6. Its first and second nodes are linked with the third one only forming a star-like structure and the first FS-cluster. The fifth, sixth and seventh nodes form the second FS-cluster. The top left block of the corresponding Jacobian matrix has the form, see Eq. (10):

$$\mathbf{F} = \begin{pmatrix} G_1\epsilon' & 0 & G_1\epsilon & 0 & 0 & 0 & 0 \\ 0 & G_1\epsilon' & G_1\epsilon & 0 & 0 & 0 & 0 \\ \frac{1}{3}g_3\epsilon & \frac{1}{3}g_3\epsilon & g_3\epsilon' & \frac{1}{3}g_3\epsilon & 0 & 0 & 0 \\ 0 & 0 & \frac{1}{4}g_4\epsilon & g_4\epsilon' & \frac{1}{4}g_4\epsilon & \frac{1}{4}g_4\epsilon & \frac{1}{4}g_4\epsilon \\ 0 & 0 & 0 & G_2\epsilon & G_2\epsilon' & 0 & 0 \\ 0 & 0 & 0 & G_2\epsilon & 0 & G_2\epsilon' & 0 \\ 0 & 0 & 0 & G_2\epsilon & 0 & 0 & G_2\epsilon' \end{pmatrix} \quad (14)$$

where  $\epsilon' = 1 - \epsilon$ ,  $g_i$  are elements of the matrix  $(-2\mathbf{G})$ , see Eq. (11), and  $g_1 = g_2 = G_1$ ,  $g_5 = g_6 = g_7 = G_2$  correspond to FS-clusters.

Due to the special form of  $\mathbf{F}$  there exist vectors of three types, whose structure is preserved under the mapping

with  $\mathbf{F}$ :

$$\vec{v}^{(0)} = \left( v_1^{(0)}, v_2^{(0)}, v_3^{(0)}, v_4^{(0)}, v_5^{(0)}, v_6^{(0)}, v_7^{(0)} \right)^T, \quad (15)$$

$$v_1^{(0)} = v_2^{(0)}, v_5^{(0)} = v_6^{(0)} = v_7^{(0)},$$

$$\vec{v}^{(1)} = \left( v_1^{(1)}, v_2^{(1)}, 0, 0, 0, 0, 0 \right)^T, \quad (16)$$

$$v_2^{(1)} + v_1^{(1)} = 1,$$

$$\vec{v}^{(2)} = \left( 0, 0, 0, 0, v_5^{(2)}, v_6^{(2)}, v_7^{(2)} \right)^T, \quad (17)$$

$$v_5^{(2)} + v_6^{(2)} + v_7^{(2)} = 0.$$

The subspaces spanned by these vectors,  $\mathbb{F}_j = \text{span}\{\vec{v}^{(j)}\}$ , where  $j = 0, 1, 2$ , are invariant with respect to  $\mathbf{F}$  and thus form the eigen-subspaces of  $\mathbf{F}$ . Moreover any vector of the form  $\vec{v}^{(1)}$  and  $\vec{v}^{(2)}$  is the eigenvector of  $\mathbf{F}$  with the eigenvalues  $G_{1,2}(1 - \epsilon)$ . Notice that all these three subspaces are pairwise orthogonal, i.e., the orthogonal are any two vectors from these subspaces.

The full Jacobian matrix  $\mathbf{J}$ , see Eq. (10), also has three eigen-subspaces  $\mathbb{J}_j = \text{span}\{\vec{w}^{(j)}\}$  spanned by the following block vectors

$$\vec{w}^{(j)} = \begin{pmatrix} \vec{v}_x^{(j)} \\ \vec{v}_y^{(j)} \end{pmatrix}, \quad (18)$$

$j = 0, 1, 2$ . Here  $\vec{v}_x^{(j)}$  and  $\vec{v}_y^{(j)}$  are the vectors with the structures (15)-(17), related to perturbations to  $x$  and  $y$  components of the system. The dimensions of these subspaces are twice the dimensions of the eigen-subspaces of  $\mathbf{F}$ . One can find explicitly a couple of corresponding eigenvectors for subspaces  $\mathbb{J}_1$  and  $\mathbb{J}_2$ :

$$\vec{w}_\pm^{(j)} = \vec{v}^{(j)} \begin{pmatrix} 1 \\ \beta/\mu_\pm^{(j)} \end{pmatrix}, \quad (19)$$

where  $\vec{v}^{(j)}$ ,  $j = 1, 2$ , are arbitrary vectors with the structure (16) and (17), respectively, and  $\mu_\pm^{(j)}$  are the corresponding eigenvalues,

$$\mu_\pm^{(j)} = \left( G_j(1 - \epsilon) \pm \sqrt{G_j^2(1 - \epsilon)^2 + 4\beta} \right) / 2. \quad (20)$$

For the considered toy network the eigenvalues  $\mu_+^{(1)}$  and  $\mu_-^{(1)}$  both have the multiplicity 1, and the multiplicity of  $\mu_+^{(2)}$  and  $\mu_-^{(2)}$  is 2.

The subspaces  $\mathbb{J}_1$  and  $\mathbb{J}_2$  include perturbations transverse to invariant manifolds of FS-clusters. The dimensions of these subspaces are 2 and 4, respectively. All vectors from  $\mathbb{J}_0$  contain identical values at sites corresponding to the same FS-cluster, see Eq. (15). It means that these vectors describe perturbations longitudinal to FS-cluster manifolds also affecting non cluster nodes. The dimension of  $\mathbb{J}_0$  is 8. All three subspaces are orthogonal to each other.

In general case the tangent space of the dynamical network under consideration is split into a set of eigensubspaces  $\mathbb{J}_j$  of  $\mathbf{J}$ , where  $0 \leq j \leq N_f$ , and  $N_f$  is the number of FS-clusters. These subspaces are time invariant and pairwise orthogonal. The subspace  $\mathbb{J}_j$ , where  $j \geq 1$ , represents perturbations transverse to the  $j$ th cluster. It is spanned by vectors having only  $2S_j$  nonzero sites corresponding to  $x$  and  $y$  variables at cluster nodes, where  $S_j$  is the size of the cluster. Since the sums along  $x$  and along  $y$  sites have to be zero, the dimension of this subspace, i.e., the number of independent vectors, is  $2(S_j - 1)$ . The subspace  $\mathbb{J}_0$  is spanned by vectors of longitudinal perturbations to FS-clusters. These vectors have identical values at sites corresponding to each node and independent values at other sites. The dimension of this subspace is  $2(N - M_f + N_f)$ , where  $M_f$  is the total number of nodes belonging to all FS-clusters.

#### IV. NONWANDERING LOCALIZATION OF CLVs ON FS-CLUSTERS

##### A. The mechanism of localization

Let  $\mathbf{\Gamma}(t)$  be a  $2N \times 2N$  matrix whose columns are CLVs at time  $t$ . By the definition, this is a unique set of vectors such that for any  $t$  the Jacobian matrix  $\mathbf{J}(t)$  maps  $\mathbf{\Gamma}(t)$  to  $[\mathbf{C}(t+1)\mathbf{\Gamma}(t+1)]$ , where  $\mathbf{C}(t)$  is a diagonal matrix logarithms of whose elements are finite time Lyapunov exponents [15]. In the other words, the tangent space operator, that is  $\mathbf{J}$  for discrete time systems, maps each CLV at  $t$  to the stretched or contracted CLV at  $t+1$ .

The direct sum of the subspaces  $\mathbb{J}_j$ ,  $0 \leq j \leq N_f$ , is equal to the whole tangent space, the subspaces are time invariant and moreover pairwise orthogonal. Thus each of them holds a set of CLVs related to perturbations to individual clusters or to non-cluster nodes. The number of these vectors is equal to the dimension of the corresponding subspace  $\mathbb{J}_j$ . These CLVs can freely evolve only within their subspaces and never leave them. Let us assume that this is not the case and there exists a probe CLV not fully belonging to one of the subspaces  $\mathbb{J}_j$ . This vector can always be decomposed into a linear combination of vectors from  $\mathbb{J}_j$ . In course of the evolution the vectors of this decomposition grow or decay exponentially, on average, but always stay within their subspaces. The rates of this growth or decay are the Lyapunov exponents. One of the vectors with the largest Lyapunov exponent will always dominate all others so that our probe CLV will fall into the corresponding subspace. Thus each CLV indeed belongs to one of  $\mathbb{J}_j$ . In principle, however, the Lyapunov exponents from different subspaces can coincide. In this case the corresponding CLVs will be linear combinations of vectors from these subspaces.

The CLVs related to transverse perturbations of FS-clusters have nonzero elements only at sites corresponding to the cluster nodes. Since the considered FS-clusters are small, the corresponding CLVs are highly localized.

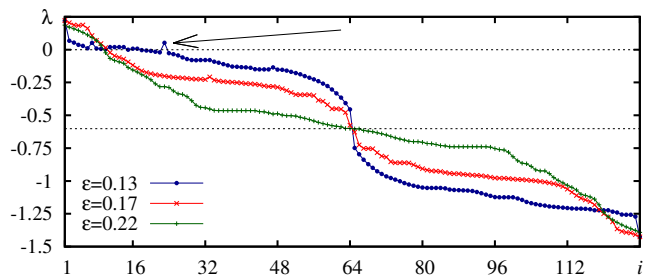


Figure 7. (color online) Lyapunov spectra of the network (1) with various coupling strengths,  $\epsilon = 0.13, 0.17,$  and  $0.22$ . The upper dotted line marks zero, while the lower one is the symmetry axis at  $(\log \beta)/2$ . The arrow points an example of anomalous behaviour.  $N = 64$ .

Moreover, this localization is nonwandering, i.e., the nonzero vector elements always have a fixed location.

Localization of CLVs is a well known phenomenon. However for chain-like systems whose nodes have identical pattern of connections the localization sites wander around irregularly from node to node [8, 9]. The nonwandering localization of CLVs is known to occur due to the inhomogeneous structure of a system. It was already reported for a disordered medium in Ref. [10]. From a general point of view the nonwandering localization of CLVs in our system also occurs because the system is highly inhomogeneous, namely, due to the star-like structures when there are highly connected hubs and low connected subordinate nodes.

##### B. Defects of Lyapunov spectra

Let us consider the Lyapunov spectra of the network (1), see Fig. 7. Observe the symmetry of the curves, emerging due to the generic symplectic structure of the Jacobian matrix, see Eq. (13). The theory behind the algorithm for Lyapunov exponents [13, 14] is based on the hierarchy of domination of tangent vectors obeyed by different Lyapunov exponents. During the computation we evolve a set of tangent vectors mapping them with the Jacobian matrix and thus allowing to align along the most expanding available directions. To exclude the alignment of all the vectors along the same directions, we periodically orthogonalize them. So the first one points the most expanding direction, the second one, as well as all others, are orthogonal to it and can only align along the second expanding direction and so on. The average exponential growth rates of these vectors are the Lyapunov exponents. Obviously they have to appear a non-ascending order.

However, in our case the non-ascending order can be broken, see the arrow in Fig. 7. Notice the absence of the symmetrical defect on the second part of the spectrum. This abnormal behaviour is related to the splitting of the tangent space into the orthogonal subspaces  $\mathbb{J}_j$ . Right af-

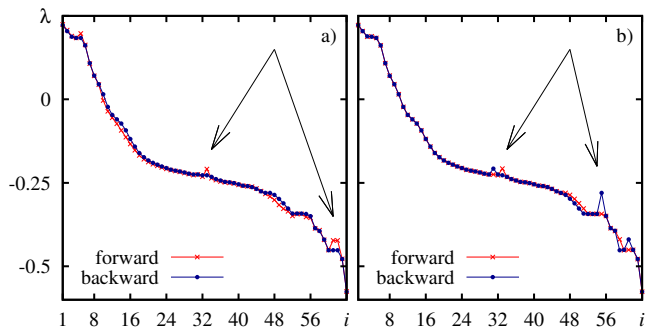


Figure 8. Lyapunov spectra computed in parallel with computation of CLVs via (a) IR- and (b) LU-methods. Two curves in the panels correspond to the exponents computed in course of forward- and backward-time stages. The arrows point the areas of essential deviations of the curves from each other.

ter the start of the iterations, the tangent vectors have random directions. If the local expansion rates for some of the subspaces  $\mathbb{J}_j$  highly deviate from the corresponding Lyapunov exponents, this subspace can attract wrong vectors. In “normal” situation the wrong orientation of vectors is fixed after a transient time when the influence of local rates decays. But in our case, since the subspaces  $\mathbb{J}_j$  are time invariant, the vectors can be trapped within inappropriate subspaces. As a result we observe the broken order of Lyapunov exponents as pointed by the arrow in Fig. 7.

One can try to avoid this trapping by adding a small noise to tangent vectors after each iteration. The noise is expected to push out the vectors from their traps giving them a chance to arrive at the appropriate subspace. Our tests showed that even very small noise of the order  $10^{-10}$  can smoothen the defects of Lyapunov spectra. However, instead of the pushing out of the trapped vectors, the noise destroys the splitting of the tangent space at all. The vectors do not gain the structures described by Eqs. (15)- (17) any more. Thus this is inappropriate approach since the existence of the tangent subspaces  $\mathbb{J}_j$  is one of the essential features of our system.

### C. Structure of CLVs

Now we turn to the CLVs. There are two numerical methods for computing CLVs whose ideas were published simultaneously. The method reported in Ref. [5] shall be referred below as IR-method. It computes CLVs in course of iterations backward in time with inverted upper triangle matrices  $\mathbf{R}$  previously obtained on the forward-time stage as a result of so called QR matrix decompositions. The other method first reported in Ref. [6] was later improved in Ref. [9] and then it was reformulated in a more efficient form in Ref. [15]. This method shall be referred as LU-method since it computes CLVs as a result of LU decomposition of matrices of scalar prod-

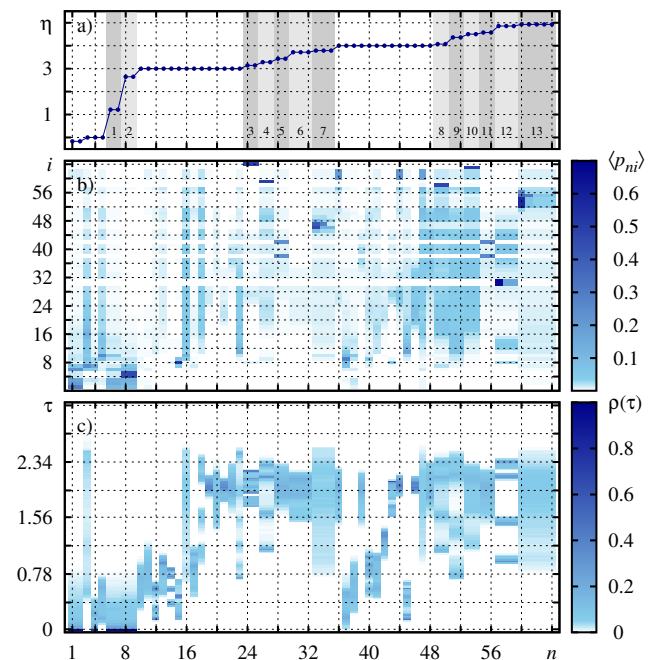


Figure 9. (color online) (a) Clustering index  $\eta_n$ , see Eq. (9). The nodes are enumerated according to the ascending order of  $\eta_n$ . Grey labeled stripes indicate FS-clusters. (b) Average node related CLVs. (c) Distributions of  $\tau_n$ , see Eq. (23). For all panel  $n$  is node number and  $i$  is the vector number.  $N = 64$ ,  $\epsilon = 0.17$ . The matrix  $\mathbf{A}$  and initial conditions are the same as in Fig. 5.

ucts of orthogonal Lyapunov vectors computed in course of forward- and backward-time procedures.

Both of the methods for CLVs includes the iterations with tangent vectors forward and backward in time. To compute CLVs correctly these iterations have to provide the identical orderings of tangent vectors, even if this does not correspond to the non-ascending order of the Lyapunov exponents. Unfortunately the trapping of vectors within inappropriate subspaces  $\mathbb{J}_j$  can occur independently and thus differently on forward and backward stages. These situations can be identified by comparing Lyapunov exponents computed in parallel with forward and backward stages, see Fig. 8. One can see that besides natural small and smooth deviations, related to an unavoidable numerical noise, there are points marked by arrows where the orders of the exponents do not coincide. It indicates that the forward- and backward-time data do not exactly match so that the corresponding CLVs are not quite correct. These abnormal deviations of the curves are found to be less pronounced for the IR method, and below we shall use it to for computing CLVs.

Figure 9(b) shows CLVs averaged in time. Since two variables are associated with each node, we consider the node related CLVs  $p_{ni} = \gamma_{2n-1,i}^2 + \gamma_{2n,i}^2$ , where  $\gamma_{ji}$  is the  $j$ th element of the  $i$ th CLV,  $i, j = 1, \dots, 2N$ ,  $n = 1, \dots, N$ . Because each CLV has a unit length,  $\sum_{n=1}^N p_{ni} = 1$  for any  $i$ . Figure 9 corresponds to the

network shown in Fig. 5. The nodes of the network are enumerated according to the ascending order of  $\eta_n$ , see Eq. (9). The curve  $\eta_n$  is shown in Fig. 9(a). Grey stripes in this panel mark FS-clusters.

According the discussion above, there are CLVs localized of FS-clusters. The most clear examples correspond to the clusters 3,4,7,8,10,12, and 13. The number of vectors has to be one less then the number of nodes in the cluster (notice that only the first part of the symmetric spectrum is shown, one more set of vectors also exist in the second part). Thus each of two-node clusters 3,4,8,and 10 produces a single localized CLV. The three-node clusters 7 and 12 generate pairs of CLVs. Finally, the five-node cluster 13 are characterized by four CLVs.

The two-node clusters 5 and 11 generate two CLVs, localized simultaneously on both of these cluster. These clusters includes the nodes {28, 29} and {55,56}, respectively. As we already discussed above, they demonstrate remote synchronization of the second order, since the nodes 28 and 29 are synchronized through the nodes 55 and 56, see Fig. 5. Due to this reason the exponential growth rates in the subspaces corresponding to these two clusters are always identical and no one of them dominates. The resulting CLVs are linear combinations of vectors localized on these clusters.

The clusters 1, 2, 6, and 9 are problematic. The two-node cluster 2 has two localized CLV instead of the expected one, and the clusters 1,6, and 9 do not have any clearly localized CLVs. We address this issues to the fails of the numerical methods due to the trapping of tangent vectors within inappropriate subspaces  $\mathbb{J}_j$ , see the discussion above.

All CLVs not localized on FS-clusters belong to  $\mathbb{J}_0$  representing longitudinal perturbations to these clusters. It means that they have to have identical values at sites corresponding to FS-clusters. One can see that this requirement is fulfilled well even for problematic clusters.

## V. NONWANDERING LOCALIZATION OF CLVs ON NODES SEPARATED FROM Ph-CLUSTERS

### A. Properties of localized vectors

Besides the localization on FS-clusters one can also observe in Fig. 9(b) that the first six vectors are localized on nodes 1, 2, 6-9. The common property of these nodes is that they do not belong to Ph-clusters, see Fig. 5.

To clarify it we shall detect the clusters at  $\mathcal{T} = 20$ . Since the oscillations of phase synchronized nodes are very close to periodic with the period 2, see Fig. 3, this short  $\mathcal{T}$  is the smallest reasonable value required to identify intermittent attachments and detachments of nodes to Ph-clusters. Running over the computation interval and performing serial detections of Ph-clusters we assign to each node at each time step a flag signalling whether this node belongs to a Ph-cluster or not. Also we com-

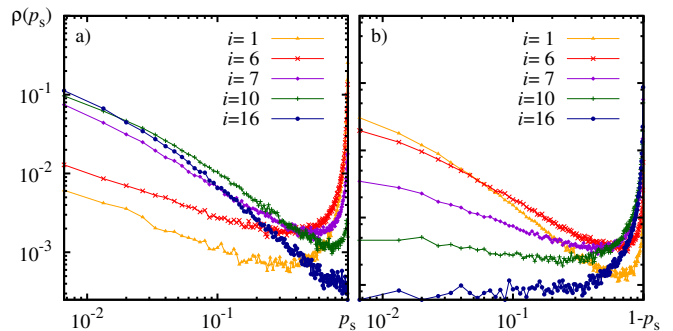


Figure 10. (color online) Power law decays of  $\rho(p_s)$  (a) near  $p_s = 0$ , and (b) near  $p_s = 1$ . Double logarithmic scales are used for both axis. The vector numbers are shown in the legends. The matrix  $\mathbf{A}$  and initial conditions are the same as in Figs. 5 and 9.

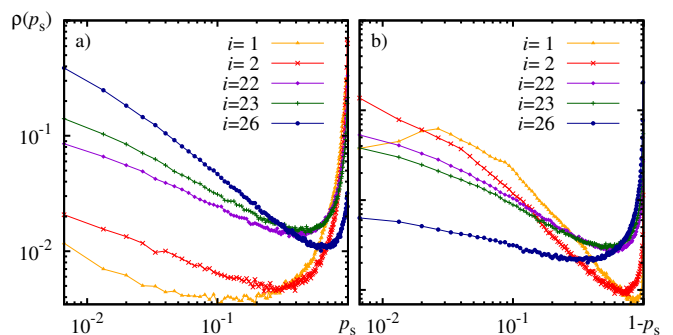


Figure 11. (color online) Distributions  $\rho(p_s)$  at  $N = 128$ ,  $\epsilon = 0.22$ .

pute CLVs and for each vector at each time step using the flags we find a sum

$$p_s(t) = \sum_{n=1}^{M_s(t)} p_{ni}(t), \quad (21)$$

where  $M_s(t)$  is the number of nodes separated from the Ph-clusters. The nodes in this equations are assumed to be enumerate in a such a way that the separated nodes go first. Since  $\sum_{n=1}^N p_{ni} = 1$ ,  $p_s$  indicates what a fraction of nonzero CLV elements belongs to the separated nodes. The upper limit  $p_s = 1$  tells that all nonzero CLV elements are localized on separated nodes, while  $p_s = 0$  shows that all nonzero CLV elements are localized on Ph-clusters.

The distributions of  $p_s$  are found to have two maxima, one at  $p_s = 0$  and the other at  $p_s = 1$ , and they decay fast towards to the middle area. Figure 10 plotted for the network in Figs. 5 and 9 shows that the decays near both edges are obeyed to power laws. Notice that the orders of the curves representing different vectors are different at the left and right edges. For the vector  $i = 1$   $\rho(0) < \rho(1)$ . It means that this vector is preferably localized on nodes not attached to the Ph-clusters. This is also the case for all vectors up to the sixth one, while for

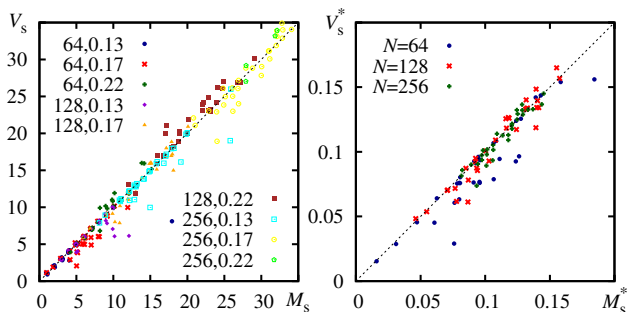


Figure 12. (color online) (a) The number of nodes non-synchronized with the Ph-clusters  $M_s$  vs. the number of CLVs  $V_s$  localized on them. The legend shows the values of  $N = 64, 128$  and  $256$  and  $\epsilon = 0.13, 0.17$ , and  $0.22$ . (b) Rescaled values  $M_s^*$  vs.  $V_s^*$ , see Eq. (22) for  $N = 64, 128$  and  $256$  at  $\epsilon = 0.17$ .

the seventh vector we observe  $\rho(0) > \rho(1)$ . Starting from this vector all other CLVs are preferably localized on the nodes attached to the Ph-clusters.

Figure 11 shows the distributions  $\rho(p_s)$  at  $N = 128$  and  $\epsilon = 0.22$ . One again observes the power laws near the edges and preferable localization of the vectors  $1 \leq i \leq 22$  on the nodes not attached to the Ph-clusters, since for these vectors  $\rho(0) < \rho(1)$ . Also notice the essential deviation from the power law of the distribution for  $i = 1$  near the right edge, see Fig. 11(b). This is the result of our approaching of  $\epsilon$  to the right boundary of the area of our consideration marked in Figs. 1 and 2. We tested more distributions at  $\epsilon = 0.24$  and observed that the deviation from the power law near  $p_s = 1$  gets higher. But nevertheless we still can distinguish the CLVs localized on separated nodes by comparing the edge values of the distributions  $\rho(0)$  and  $\rho(1)$ .

Thus the first CLVs, whose number we denote as  $V_s$ , are preferably localized on the nodes not synchronized with the Ph-clusters. Notice that due to the symmetry there are more  $V_s$  localized vectors in the opposite end of the spectrum.

Since these CLVs have nonzero values mainly on a limited and permanent set of nodes whose number we denote as  $M_s$ , the number of these vectors have to be at least approximately equal to the number of these nodes,  $V_s \approx M_s$ . To verify it we generate different matrices  $\mathbf{A}$  and find the separated nodes for it. Then we find CLVs and compute the relative frequency  $P(p_s > 0.5)$ , where  $p_s$  is computed as discussed above, see Eq. (21). The vector is treated as localized on the separated nodes when  $P > 0.5$ . The number of such vectors  $V_s$  as a function of the number of separated nodes  $M_s$  is plotted in Fig. 12. Since  $M_s$  and  $V_s$  are integer, the points of the plot will overlap each other. To avoid it and show the areas where the points fall more often as dense clouds we add random numbers  $\xi \in (-0.2, 0.2)$  to data:  $M_s + \xi$  and  $V_s + \xi$ . Panel (a) shows nine data sets computed at  $\epsilon = 0.13, 0.17$ , and  $0.22$  for  $N = 64, 128$ , and  $256$ . The points are fitted very well by the straight line  $V_s = M_s$  that confirms the ex-

pected relation between the number of localized vectors and the number of separated nodes.

Figure 12(b) illustrates the scaling of  $M_s$  and  $V_s$  with the network size  $N$ . One sees that though different matrices  $\mathbf{A}$  result in different  $M_s$  and  $V_s$ , the scaling

$$M_s^* = M_s/N, \quad V_s^* = V_s/N, \quad (22)$$

results in the gathering of points withing the same ranges. It means that the number of nodes separated from the Ph-clusters as well as the number of localized on them CLVs grow with  $N$  as  $M_s \sim N$ , and  $V_s \sim N$ . Notice that this agrees with previously discussed scaling of the number of nodes attached to the Ph-clusters, see Eq. (7).

We also checked the signs of Lyapunov exponents corresponding to the localized CLVs. In all cases the localized CLVs had positive Lyapunov exponents and the total number of positive Lyapunov exponents was always higher then  $V_s$ .

## B. Properties of localization nodes

The separated nodes where the first CLVs are localized have common specific feature related to the instantaneous square deviations of a node from its neighborhood:

$$\tau_n(t) = h_n^2(t). \quad (23)$$

where  $h_n(t)$  is given by Eq. (2). Figure 9(c) shows the distributions of  $\tau_n$ . One can see that the distributions at nodes 1, 2, 6-9 have the maximum in zero and they decay monotonically. On contrary, the distributions at nodes with numbers  $n \geq 10$  are quite different: all of them are separated from zero, and in some cases they are multimodal.

Since nodes 3, 4, and 5 are the floating ones, as indicate corresponding values of  $\eta_n$  in Fig. 9(a), the forms of corresponding distributions of  $\tau_n$  are ambiguous. On the one hand side, the distribution at node 4 looks as in non-floating ones. However, the distributions in nodes 3 and 5 correspond to the situation when a node belong to a Ph-cluster at  $n \geq 10$ .

This can be clarified by finding the clusters at short interval,  $\mathcal{T} = 20$ . Performing the serial cluster detections with this  $\mathcal{T}$  for the network in Figs. 5 and 9 we found that the separated nodes 1 and 2 as well as the nodes of the small FS-clusters 6-9 can sometimes be attached to a Ph-cluster, but approximately 90% of time they oscillate separately. Contrary to this the floating node 3 is not synchronized with the Ph-clusters only 0.0008% of time steps, and node 5 is separated 0.0002% of time. However the node 4 remains separated from Ph-clusters during 0.0022% of time steps. Though this is still a very small value but it is one order higher then for the nodes 3 and 5. Thus the form of the distribution of  $\tau_n$  depends on the percentage of time that the node spends being not synchronized with the Ph-clusters.

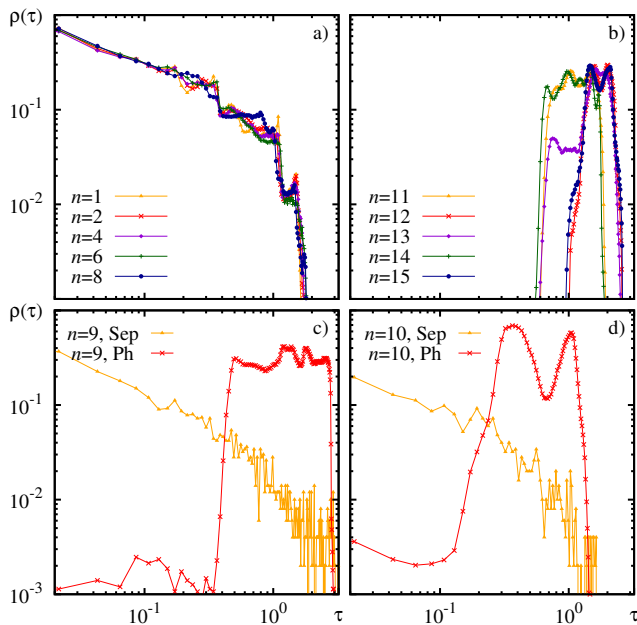


Figure 13. (color online) Distributions  $\rho(\tau)$  at  $N = 128$ ,  $\epsilon = 0.13$  at different nodes  $n$ . The nodes are enumerated according to the growth of  $\eta_n$ , see Eq. (9). Panel (a) shows the separated nodes, while panel (b) corresponds to the nodes attached to the Ph-clusters. Panels (c) and (d) demonstrate distributions at the floating nodes  $n = 9$  and  $10$ , respectively, computed independently when the node is separated (label “Sep” in the legend) and attached to the Ph-clusters (label “Ph”).

Figure 13 exemplifies the typical forms of the distributions of  $\tau_n$  in more detail. A network generated to plot this figure had eight purely separated nodes and two floating ones. The nodes are assumed to be enumerated according to the growth of clustering index  $\eta_m$ , see Eq. (9). In panel (a) one can see that the distributions of  $\tau_n$  at the separated nodes have power law shape near the origin, right after that it decays to zero, and moreover the shapes of distributions in all of these nodes are almost identical. On contrary, the distributions at Ph-cluster nodes are well separated from zero and can have multiple maxima, see panel (b). To plot the distribution for floating nodes in panels (c) and (d) we collected the data in two arrays, one was used when the node was attached to a Ph-cluster, and the other when it was separated. One can see that oscillating separately the floating node demonstrate the power law distribution of  $\tau_n$ . The exponent coincides with the exponents of the distributions for purely separated nodes, cf. the slopes of the curves in panels (a) with the slopes of the corresponding curves in panels (c) and (d). When the floating node is attached to a Ph-cluster its distribution corresponds in bulk to the distributions at purely cluster nodes, cf. the curves in panel (b) with the corresponding curves in panels (c) and (d). However a remnant power law tail near the origin can also be observed in panel (d).

One can see in Fig. 5 that each of the separated nodes where the first CLVs are localized has only one connection. This is typical for the localization nodes. Computing the connectivity degrees  $k_n$  in parallel with the data for Fig. 12 we found that in the most cases  $k_n = 1$  though rarely it can be higher. Nevertheless, the average connectivity degree of the separated nodes where CLVs are localized is less than 2.

Altogether, the first  $V_s$  CLVs are localized on  $M_s$  nodes. These nodes have specific properties: they are not synchronized with large Ph-clusters, in most cases they have only one connection, and the distributions of  $\tau_n$  at these nodes have identical power law shapes. The core set of these nodes remains unchanged in course of the dynamics (however there can exist a few so called floating nodes). It means that this localization of CLVs is nonwandering. Since the localization nodes can be found without the straightforward computation of CLVs, we can predict where the first  $V_s$  CLVs are localized.

## VI. SUMMARY AND CONCLUSION

In this paper we found that CLVs for a dynamical network can demonstrate nonwandering localization on nodes that can be found without the computation of CLVs. This is an example of explicit relations between dynamics of a system and the associated tangent space dynamics.

Random scale-free dynamical networks of Hénon maps are considered. The networks are generated using preferential attachment mechanism, and the resulting network always have  $N$  nodes and  $N - 1$  connections.

The dynamics of such network is chaotic. Though the synchronization of the whole network is not observed, the nodes can form synchronized clusters. Full chaotic synchronization as well as phase synchronization are possible. The number of clusters depend on the coupling strength. We limit ourselves with a range of coupling strengths where there are two large phase clusters including together almost all nodes, and many small fully synchronized clusters. Most of them are embedded into the phase clusters while several ones can be separated.

Due to the presence of clusters, covariant Lyapunov vectors are found to be localized. Each cluster of  $S_f$  fully synchronized nodes is associated with  $2(S_f - 1)$  covariant vectors all of whose sites are strictly zeros except for the nodes corresponding to the clusters. This localization is nonwandering and predictable since we can find nonzero vector sites without computing the covariant vectors. However it is unclear which vector will be localized on the particular cluster.

One more mechanism of localization is related to the phase clusters. The first  $V_s$  CLVs are localized on  $M_s$  nodes that oscillate separately from the phase clusters. This localization is not quite strict as the previous one, and the vectors can have nonzero sites on nodes attached to the phase clusters. But the probability of localization

on separated nodes is always higher and this is the criterion for distinguishing of these vectors. The number of vectors  $V_s$  and the number of separated nodes  $M_s$  are equal, however since the localization is not strict this equality is approximate. As well as the localization of clusters of full synchronization this is the nonwandering and predictable localization. Finding the nodes oscillating separately from the phase clusters we can say in advance where the first CLVs will be preferably localized and what will be their number. The nodes of localization have specific features: they are very low connected (only one connection, in the most cases), and they demonstrate identical power law distributions of square deviations of dynamical variables from their neighborhood.

The a priori knowledge about the localization of the covariant vectors opens perspectives of wider utilizing of these vectors. By the definition these vectors show how

the development of perturbations occurs. When the locations of areas of the most intensive development is permanent and predictable, the interesting problem arises to organize an effective low energy forcing to the system using this areas.

Computing CLVs for the dynamical networks with full synchronization clusters we found that both known methods can be not quite correct due the splitting of the tangent space into a set of time invariant pairwise orthogonal subspaces. In view of the great interest of researcher to the dynamical networks a challenging task emerges to modify the numerical methods for CLVs to fix this problem.

PK thank U. Parlitz for stimulating discussions.

PK acknowledges the President RF program of support of leading Russian research schools NSh-1726.2014.2.

- 
- [1] K. Kaneko, “Lyapunov analysis and information flow in coupled map lattices,” *Physica D* **23**, 436 – 447 (1986).
- [2] G. Giacomelli and A. Politi, “Spatio-temporal chaos and localization,” *Europhys. Lett.* **15**, 387 (1991).
- [3] M. Falcioni, U. Marini Bettolo Marconi, and A. Vulpiani, “Ergodic properties of high-dimensional symplectic maps,” *Phys. Rev. A* **44**, 2263–2270 (1991).
- [4] G. P. Morriss, “Localization properties of covariant lyapunov vectors for quasi-one-dimensional hard disks,” *Phys. Rev. E* **85**, 056219 (2012).
- [5] F. Ginelli, P. Poggi, A. Turchi, H. Chaté, R. Livi, and A. Politi, “Characterizing dynamics with covariant lyapunov vectors,” *Phys. Rev. Lett.* **99**, 130601 (2007).
- [6] C. L. Wolfe and R. M. Samelson, “An efficient method for recovering lyapunov vectors from singular vectors,” *Tellus A* **59**, 355–366 (2007).
- [7] R. Buizza and T. N. Palmer, “The singular-vector structure of the atmospheric global circulation,” *J. Atmos. Sci.* **52**, 1434–1456 (1995).
- [8] Arkady S. Pikovsky and Jürgen Kurths, “Roughening interfaces in the dynamics of perturbations of spatiotemporal chaos,” *Phys. Rev. E* **49**, 898–901 (1994); A. Pikovsky and A. Politi, “Dynamic localization of lyapunov vectors in spacetime chaos,” *Nonlinearity* **11**, 1049 (1998).
- [9] D. Pazó, I. G. Szendro, J. M. López, and M. A. Rodríguez, “Structure of characteristic lyapunov vectors in spatiotemporal chaos,” *Phys. Rev. E* **78**, 016209 (2008).
- [10] I. G. Szendro, J. M. López, and M. A. Rodríguez, “Dynamics of perturbations in disordered chaotic systems,” *Phys. Rev. E* **78**, 036202 (2008).
- [11] A. Politi and A. Torcini, “Periodic orbits in coupled Hénon maps: Lyapunov and multifractal analysis,” *Chaos* **2**, 293–300 (1992).
- [12] A.-L. Barabási, R. Albert, and H. Jeong, “Scale-free characteristics of random networks: the topology of the world-wide web,” *Physica A* **281**, 69 – 77 (2000).
- [13] G. Benettin, L. Galgani, A. Giorgilli, and J. M. Strelcyn, “Lyapunov characteristic exponents for smooth dynamical systems and for hamiltonian systems: A method for computing all of them. Part I: Theory. Part II: Numerical application,” *Meccanica* **15**, 9–30 (1980).
- [14] I. Shimada and T. Nagashima, “A numerical approach to ergodic problem of dissipative dynamical systems,” *Prog. Theor. Phys.* **61**, 1605–1616 (1979).
- [15] P. V. Kuptsov and U. Parlitz, “Theory and computation of covariant Lyapunov vectors,” *J. Nonlinear Sci.* **22**, 727–762 (2012).
- [16] Sarika Jalan and R. E. Amritkar, “Self-organized and driven phase synchronization in coupled maps,” *Phys. Rev. Lett.* **90**, 014101 (2003); S. Jalan, R. E. Amritkar, and Ch.-K. Hu, “Synchronized clusters in coupled map networks. i. numerical studies,” *Phys. Rev. E* **72**, 016211 (2005).
- [17] A. Bergner, M. Frasca, G. Sciuto, A. Buscarino, E. J. Ngamga, L. Fortuna, and J. Kurths, “Remote synchronization in star networks,” *Phys. Rev. E* **85**, 026208 (2012).
- [18] L. V. Gambuzza, A. Cardillo, A. Fiasconaro, L. Fortuna J. Gomez-Gardenes, and M. Frasca, “Analysis of remote synchronization in complex networks,” *Chaos* **23**, 043103 (2013).
- [19] Ute Dressler, “Symmetry property of the lyapunov spectra of a class of dissipative dynamical systems with viscous damping,” *Phys. Rev. A* **38**, 2103–2109 (1988).
- [20] A. J. Bosch, “The factorization of a square matrix into two symmetric matrices,” *Am. Math. Month.* **93**, 462–464 (1986).